Recent Progress on a Radon Detector with Electrostatic Collection

Yuuki Nakano[a)]

Kamioka Observatory, Institute for Cosmic Ray Research, the University of Tokyo, Gifu 506-1205, Japan

[a)]*Corresponding author: ynakano@km.icrr.u-tokyo.ac.jp*

Abstract. In the field of particle physics, various experiments have been designed in order to search for rare physics processes beyond the standard model. The radioactive noble gas radon is one of the major background sources below the MeV region in rare-event search experiments. To precisely monitor the radon concentration in purified gases, radon detectors with electrostatic collection are widely used. To extend the application of the Rn detector, we have constructed a calibration system in the Kamioka underground laboratory and evaluated the detector performance by filling the Rn detector with various gases, such as purified air, argon, xenon, and tetrafluoromethane. In these proceedings, we overview the recent progress of the Rn detector development, its performance with various gases, and a Rn removal test using activated carbon fibers.

INTRODUCTION

Over the last 40 years, the standard model of particle physics has demonstrated huge successes in providing experimental predictions, which have been experimentally confirmed with high precision. In the field of particle physics, various experiments have been designed in order to search for rare physics processes beyond the standard model. As a target for dark matter or neutrino interactions, or as a source for neutrino-less double beta ($0\nu2\beta$) decay, a material is carefully selected depending on its nuclear characteristics, such as spin structure, mass number, and chemical properties. For example, the noble gas xenon (Xe) is widely used for a target nucleus to search for Weakly Interacting Massive Particle (WIMPs) due to its relatively large mass and spin properties [1, 2, 3, 4, 5], and for a source of $0\nu2\beta$ decay [6, 7, 8]. Argon (Ar) is also used as a target nucleus for WIMP searches [9, 10, 11] and for neutrino interactions [12, 13] because of its scintillation properties. In addition, fluorine (F) compounds (such as Octafluoropropane (C_3F_8 [14]), tetrafluoromethane (CF_4 [15, 16]), and sulfur hexafluoride (SF_6 [17, 18])) attract significant attention for WIMP searches because of fluorine's large cross section for a spin-dependent interaction [19].

Backgrounds in the Experiments Searching for Rare Physics Processes

Although natural Ar, Xe, and F do not have intrinsic long-lived isotopes [20], experiments searching for rare processes suffer from radioactive impurities that exist in their target in gas or liquid states. Such radioactive decays limit a detector's sensitivity below the multi-MeV region. In particular, the noble gas radon (^{222}Rn) is continuously produced from the decay of radium (^{226}Ra) in the uranium (^{238}U) chain in materials used for the detector components. Hence, background controls are required to keep the detector's background level low, for example material screenings before the detector construction [21, 22] and purification techniques during operations [23, 24, 25].

For monitoring, a Rn detector with a PIN-photodiode has been developed over the last 50 years. The latest type of Rn detector can precisely measure the Rn concentration in purified gas with an accuracy of 1 mBq/m^3 in a single day measurement [26]. In these proceedings, we briefly overview the recent progress of studies related with the Rn detector with the electrostatic collection based on Ref. [26, 27, 28]. In addition to the development status, we also report the test of Rn removal from purified gas with activated carbon fibers (ACF) based on [29, 30].

RADON DETECTOR

The Rn detector consists of an 80-liter stainless steel vessel, a PIN-photodiode, a ceramic feedthrough, and an electrical circuit. The PIN-photodiode is connected to the inner end of the feedthrough, which is mounted on the top flange of the vessel. The high-voltage divider and readout electronics [31] are also connected to the external end of the feedthrough. We have originally used the PIN-photodiode whose size is 18×18 mm and newly used the larger

one whose size is 28×28 mm in this study. In order to reduce the intrinsic background from the detector components, the inner surface of the Rn detector is electropolished [27].

The principal technique of such Rn detectors is electrostatic collection [32]. Because the daughter nuclei of ^{222}Rn tend to be positively charged [33], they are easily collected by forming an electrical field inside the detector. The PIN-photodiode, where charged nuclei are collected, uniquely identifies the energy of the α particle emitted via the daughter's subsequent decays because of its high spectral resolution.

Humidity in the filled gas makes the positively charged nuclei neutralized, resulting in collection inefficiency [34, 35]. To improve the collection efficiency, we replaced the original, 18×18 mm PIN-photodiode with a larger, 28×28 mm one and compared the detector performance with [28]. This replacement enables the detector to enlarge the volume where the electrical field is formed, and to improve the collection efficiency of positively charged particles.

CALIBRATION SYSTEM AND RESULTS

For evaluating the improvement of the measurement sensitivity by replacing the large sized PIN-photodiode, we constructed a calibration setup at Lab-A in the experimental area at Kamioka Observatory. The calibration system, which was also used previously in Ref. [28], consists of two 80-liter Rn detector chambers, a temperature sensor, an air circulation pump, a cold trap, pressure gauges, and a mass flow controller. We installed a large PIN-photodiode in one of the two Rn detector chambers and a small PIN-photodiode in the other. We used a ^{226}Ra source, whose activity is $(199 \pm 4\%)$ Bq, to inject ^{222}Rn gas into the calibration system and to maintain radioactive equilibrium in the system.

Calibration results

For converting the count rate of ^{214}Po signal into the Rn concentration in the filling gas, the calibration factor is measured by the calibration system. Here, the calibration factor (C_F) is defined as

$$C_F = \frac{\text{Daily } ^{214}\text{Po count rate [count/day]}}{\text{Rn concentration in the calibration system [mBq/m}^3\text{]}}. \quad (1)$$

The signal efficiency $\varepsilon_{^{214}\text{Po}}$ of ^{214}Po (the fraction of ^{214}Po alpha decays that are detected) is given by

$$\varepsilon_{^{214}\text{Po}} = \frac{Z_{^{214}\text{Po}}}{(\lambda A/F)V}, \quad (2)$$

where $Z_{^{214}\text{Po}}$ is the observed count rate in the Rn detector, λ is the decay constant of ^{222}Rn, A is the Rn activity of the source, F is the flow rate of circulating gas (typically 0.6 L/min), and V is the volume of the Rn detection chamber.

Figure 1 shows the dependence of C_F as well as the signal efficiency $\varepsilon_{^{214}\text{Po}}$ of ^{214}Po on absolute humidity and high voltage, as measured by the calibration system filled with Ar gas. The results demonstrate that C_F of the Rn detector with the larger PIN-photodiode is higher than that with the small one in the dry region below 1.0 g/m^3. The results also demonstrate a clear dependence on the applied high voltage. Based on the calibration results, the total ^{214}Po signal efficiency $\varepsilon_{^{214}\text{Po}}$ is about 30% level at most, where the collection efficiency by the electrical field is about 60%.

Figure 2 shows the absolute humidity dependence of C_F as the ^{214}Po signal efficiency measured by the calibration system filled with various gases. Although the calibrations were performed under the same condition, the results demonstrate the clear differences of C_F. We are now investing a possible correlation between the collection efficiency (or C_F) and the gas's chemical properties, such as mass, polarization, and ionized potential energy.

ACTIVATED CARBON FIBER

As briefly explained in the former section, the residual Rn in the target (or source) material should be removed by a purification process during the detector's operation. In order to remove the Rn in purified gas, porous materials, such as activated carbon and molecular sieves, are widely used because their pores on the surface can capture Rn [30,

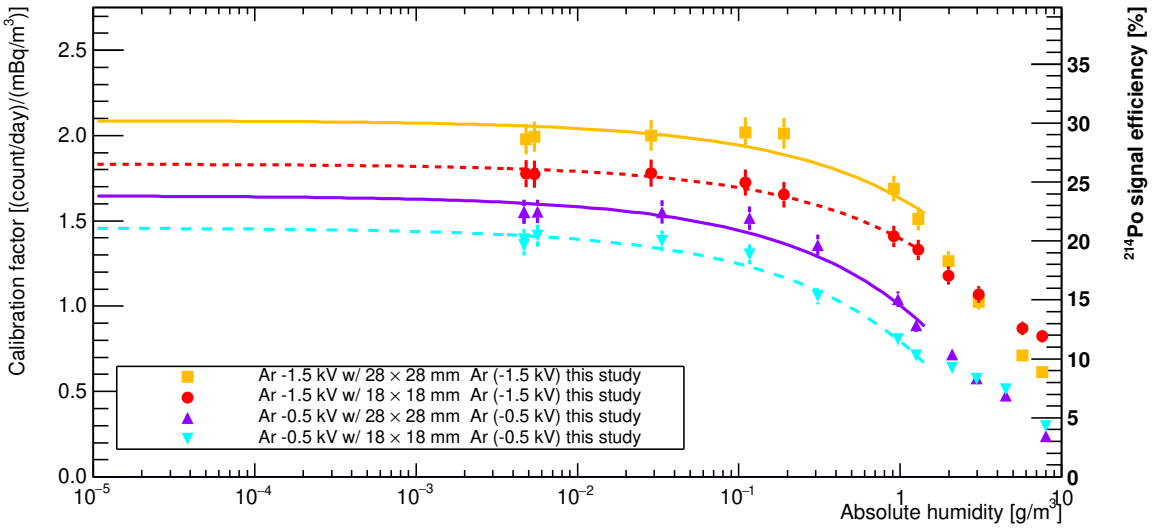

FIGURE 1. The calibration factors as well as the signal efficiencies of ^{214}Po determined by the calibration system by filling the Rn detector with purified Ar. Orange squares (red circles) show the calibration factors measured with the PIN-photodiode whose size is 28×28 mm (18×18 mm) by applying the high-voltage at -1.5 kV. Purple upward triangles (light blue downward triangles) show those at -0.5 kV. The curved lines are the fitting results with an empirical function of $A + B\sqrt{AH}$, where the parameter AH is the absolute humidity in the filling gas.

TABLE I. The basic properties of ACFs, and their intrinsic radioactivity measured with the high purity Germanium detector at Kamioka observatory, compared to other activated charcoals. The upper limit values are at the 90% confidence level. Note that we measured the late parts of the chains in Uranium and Thorium series.

Product name	Specific surface area [m^2/g]	Average pore diameter [nm]	Uranium series [mBq/kg]	Thorium series [mBq/kg]	^{40}K [mBq/kg]
A-10 [29]	1300	1.7	< 352	< 305	$< 4.31 \times 10^3$
A-15 [29]	1700	1.9	< 11.9	< 12.2	< 142
A-20 [29]	2000	2.2	< 5.5	< 10.4	< 49
A-25 [29]	2667	2.5	< 269	< 261	$< 4.31 \times 10^3$
Shirasagi G$_{2X}$ 4/6 [36]	–	–	67 ± 15 [a]	–	–
Shirasagi G$_{2X}$ 4/6 [39]	1240 [41]	–	62 ± 4 [b]	–	–
Blücher 100050 [39]	–	–	2.6 ± 0.3 [b]	–	–
CarboAct [40]	800–1200 [41]	–	< 0.3 [c]	–	–

[a] Measured with the same high purity Germanium detector at Kamioka observatory used to measure intrinsic radioactivity of A-10, A-15, A-20, and A-25 listed in this table.
[b] Measured with a proportional counter.
[c] Measured with the Rn emanation setup [42].

36, 37]. Activated charcoal is an effective adsorbent for various impurities through a physical process based on van der Waals forces and the polarizability of atoms [38]. However, when the molecule sizes of the inert gas and Rn are similar, such as with Xe, both Rn and the inert gas tend to be adsorbed by the adsorbent. Hence, the pore size of activated carbon should be selected carefully. As a first study, the Rn removal efficiencies for purified air, Ar, Xe, and CF_4 were evaluated by using the Rn detector [29, 30].

We used activated carbon fibers (ACFs), which were provided by Unitika Ltd., because these products are manufactured with aligned pore sizes (average pore diameter) on the surface [29]. Table I summarizes the basic properties of these ACFs and compares their intrinsic radioactivity with that of other activated charcoals evaluated by other groups [36, 39, 40]. For Rn removal, the carbon's intrinsic radioactivity should be as low as possible. We measured the intrinsic radioactivity with a high purity Germanium detector and found that the ACF intrinsic background level is comparable to, and sometimes lower than, other products.

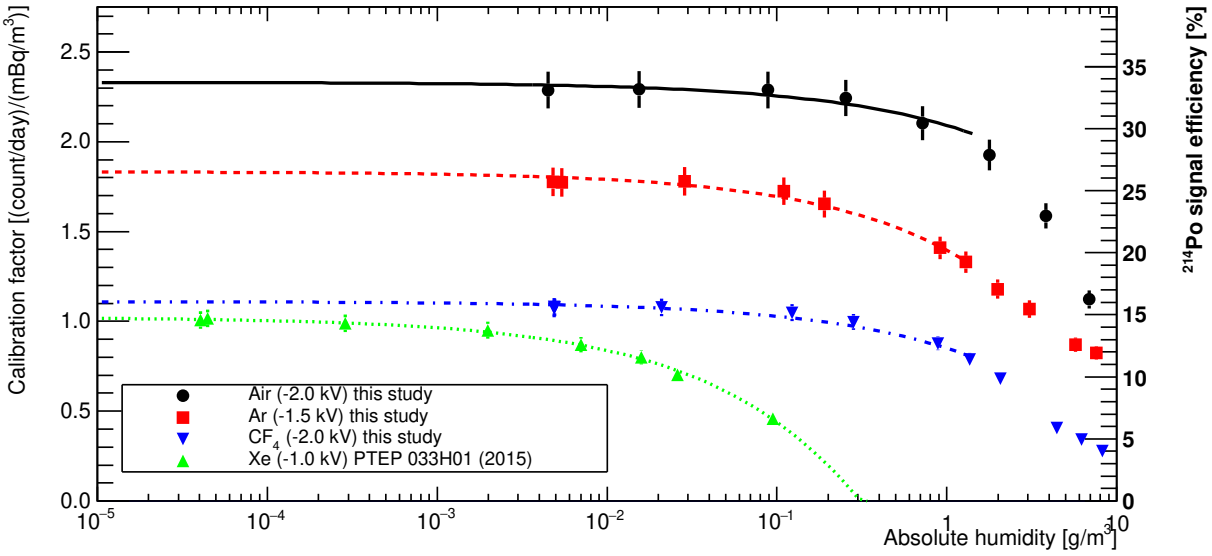

FIGURE 2. The measured calibration factors as well as the ^{214}Po signal efficiency when filling the Rn detector with purified air (black circles), Ar (red squares), and CF_4 (blue downward triangles). As a comparison, the calibration factors with Xe measured in Ref. [27] is also drawn (green upward triangles). The results shown in this figure were taken with the PIN-photodiode whose surface area is 18×18 mm. The results with the large PIN-photodiode (28×28 mm) are being prepared. In the case of CF_4 measurement, we observed the 20% level difference between the result in this study and the result shown in Ref. [30]. The result in this study was taken with the flow rate at 0.26 standard liter per minute (SLM) in Kamioka observatory. On the other hand, the result shown in Ref. [30] was taken at 0.4 SLM in Kobe university. Hence, we used different Rn detectors in two places and calibrated them with the different flow rates. Those differences may explain the discrepancy of calibration factors.

TABLE II. The measured Rn adsorption efficiencies for several gases with the ACFs evaluated with the measurement system at Kobe university [29, 30]. The σ parameter [43] of Rn is 0.417–0.421 nm, which is similar to that of Xe. The σ parameter of CF_4 is the largest among tested gases since it is a polyatomic molecule.

Gas	σ parameter [nm]	ACFs	Rn adsorption efficiency [%]	Gas flow rate [Standard liter per minute]
Purified air	0.352–0.369	A-15	$98.3 \pm 0.1\,(\text{stat.}) \pm 0.2\,(\text{syst.})$	1.3
Ar	0.340–0.346	A-15	$97.9 \pm 0.2\,(\text{stat.}) \pm 0.2\,(\text{syst.})$	0.9
Xe	0.396–0.410	A-25	$27.8 \pm 0.2\,(\text{stat.})^{+2.0}_{-5.5}\,(\text{syst.})$	0.14
CF_4	About 0.470	A-25	$82.7 \pm 0.1\,(\text{stat.}) \pm 2.3\,(\text{syst.})$	0.4

In order to evaluate the Rn removal efficiency from purified gases with the ACFs, a measurement system, which was constructed in Kobe university [29, 30], was used. The measurement system consists of the 80-liter Rn detector, a gas mass flow controller, a gas circulation pump, a dew point sensor, a pressure gauge, a filter, a refrigerator with a cold ACF trap with about 12 g of ACF, and a Rn source. At first, we filled the system with purified gas, injected some amount of Rn gas to the system, measured the Rn concentration inside the whole system except for the ACF trap with the Rn detector, and estimated the expected Rn concentration by fitting its decay curve. Then, we opened the ACF trap cooled at -90°C, measured the Rn concentration after passing through the trap, and evaluated the Rn adsorption efficiencies by comparing the measured and expected Rn concentrations, as detailed in Ref. [29]. Table II summarizes the size of the molecule, as represented by the σ parameter in the Lennard-Jones potential approximation [43], and the measurement results of Rn adsorption efficiencies.

The measurement results show the adsorption efficiencies with purified air, Ar, and CF_4 are higher than that with Xe. This is possibly due to the fact that a considerable proportion of the ^{222}Rn atoms never have a chance to be adsorbed, as they are superseded by Xe atoms, which have the closest Lennard-Jones σ parameter to ^{222}Rn, and hence are a suitable size for adsorption.

CONCLUSION AND PROSPECTS

Rn detectors with electrostatic collection are widely used for monitoring Rn concentrations in purified gases. We have constructed a calibration setup to evaluate such detectors' performance. We determined that enlarging the size of the PIN-photodiode, where the positively charged nuclei are collected, improves the efficiency of collecting Rn daughters, as expected since the volume where the electrical field is formed is enlarged. To extend the application of the Rn detector for other gases, we have evaluated several basic properties of such detectors by filling the detection chamber with several purified gases, such as purified air, argon, xenon, and tetrafluoromethane. The calibration demonstrates that the detector performance clearly depends on the type of gas. We are now investigating a possible correlation between the detector's performance and chemical properties of the tested gases. As a future work, the calibration by filling SF_6 gas is scheduled in September, 2022.

For developing techniques to remove Rn from purified gases, we tested the Rn absorption efficiency by using activated carbon fiber (ACF) provided by Unitika Ltd. The provided ACFs have relatively low intrinsic backgrounds compared with other types of adsorbents. For the test of their removal capabilities, we constructed another measurement setup and evaluated the Rn absorption efficiency with several type of ACFs by circulating the test gases. The lower adsorption efficiencies of gases with large mass compared to other carrier gases can be explained by a difference in the σ parameter in the Lennard-Jones potential.

ACKNOWLEDGMENTS

The author thanks H. Sekiya, G. Pronost, and Y. Takeuchi for their support in many aspects of this study. The author also thanks R.W. Schnee for providing valuable comments and correcting the sentences throughout these proceedings. The author gratefully acknowledges the cooperation of the Kamioka Mining and Smelting Company. This work is supported by MEXT KAKENHI Grant Numbers 18H05536, 20K03998, and 21K13942, and the inter-university research program at Institute for Cosmic Ray Research (ICRR), the University of Tokyo.

REFERENCES

1. D. S. Akerib *et al.* (The LUX collaboration), "The Large Underground Xenon (LUX) experiment," Nucl. Instrum. Meth. A **704**, 111–126 (2013), arXiv:1211.3788 [physics.ins-det].
2. E. Aprile *et al.* (The XENON100 collaboration), "The XENON100 dark matter experiment," Astropart. Phys. **35**, 573–590 (2012), arXiv:1107.2155 [astro-ph.IM].
3. K. Abe *et al.* (The XMASS collaboration), "XMASS detector," Nucl. Instrum. Meth. A **716**, 78–85 (2013), arXiv:1301.2815 [physics.ins-det].
4. X. Cao *et al.* (The PandaX collaboration), "PandaX: a liquid xenon dark matter experiment at CJPL," Sci. China Phys. Mech. Astron. **57**, 1476–1494 (2014), arXiv:1405.2882 [physics.ins-det].
5. M. Auger *et al.*, "The EXO-200 detector, part I: detector design and construction," JINST **7**, P05010 (2012), arXiv:1202.2192 [physics.ins-det].
6. A. Gando *et al.* (The KamLAND-Zen collaboration), "Search for Majorana neutrinos near the inverted mass hierarchy region with KamLAND-Zen," Phys. Rev. Lett. **117**, 082503 (2016), [Addendum: Phys. Rev. Lett. 117, 109903 (2016)], arXiv:1605.02889 [hep-ex].
7. P. Ferrario *et al.* (The NEXT collaboration), "First proof of topological signature in the high pressure xenon gas TPC with electroluminescence amplification for the NEXT experiment," JHEP **01**, 104 (2016), arXiv:1507.05902 [physics.ins-det].
8. S. Ban *et al.*, "Electroluminescence collection cell as a readout for a high energy resolution xenon gas TPC," Nucl. Instrum. Meth. A **875**, 185–192 (2017), arXiv:1701.03931 [physics.ins-det].
9. P. A. Amaudruz *et al.* (The DEAP-3600 collaboration), "Design and construction of the DEAP-3600 dark matter detector," Astropart. Phys. **108**, 1–23 (2019), arXiv:1712.01982 [astro-ph.IM].
10. T. Alexander *et al.* (The DarkSide collaboration), "DarkSide search for dark matter," JINST **8**, C11021 (2013).
11. M. Tanaka, "Status of R&D on double phase argon detector: the ANKOK project," J. Phys. Conf. Ser. **469**, 012012 (2013).
12. C. Adams *et al.* (The MicroBooNE collaboration), "Design and construction of the MicroBooNE cosmic ray tagger system," JINST **14**, P04004 (2019), arXiv:1901.02862 [physics.ins-det].
13. B. Abi *et al.* (The DUNE collaboration), "Deep Underground Neutrino Experiment (DUNE), far detector technical design report, volume IV: far detector single-phase technology," JINST **15**, T08010 (2020), arXiv:2002.03010 [physics.ins-det].
14. C. Amole *et al.* (The PICO collaboration), "Dark matter search results from the complete exposure of the PICO-60 C_3F_8 bubble chamber," Phys. Rev. D **100**, 022001 (2019), arXiv:1902.04031 [astro-ph.CO].
15. T. Tanimori, H. Kubo, K. Miuchi, T. Nagayoshi, R. Orito, A. Takada, and A. Takeda, "Detecting the WIMP-wind via spin-dependent interactions," Phys. Lett. B **578**, 241–246 (2004), arXiv:astro-ph/0310638.
16. J. B. R. Battat *et al.* (The DRIFT collaboration), "First background-free limit from a directional dark matter experiment: results from a fully fiducialised DRIFT detector," Phys. Dark Univ. **9–10**, 1–7 (2015), arXiv:1410.7821 [hep-ex].
17. N. S. Phan, R. Lafler, R. J. Lauer, E. R. Lee, D. Loomba, J. A. J. Matthews, and E. H. Miller, "The novel properties of SF_6 for directional dark matter experiments," JINST **12**, P02012 (2017), arXiv:1609.05249 [physics.ins-det].

18. T. Ikeda, T. Shimada, H. Ishiura, K. D. Nakamura, T. Nakamura, and K. Miuchi, "Development of a negative ion micro TPC detector with SF_6 gas for the directional dark matter search," JINST **15**, P07015 (2020), arXiv:2004.09706 [physics.ins-det].
19. J. R. Ellis and R. A. Flores, "Elastic supersymmetric relic - nucleus scattering revisited," Phys. Lett. B **263**, 259–266 (1991).
20. Note that ^{39}Ar is produced in the atmosphere by cosmic ray. Xe is contaminated with ^{85}Kr during manufacture and refinement. Only ^{19}F is stable and naturally occurring.
21. E. Aprile *et al.* (The XENON collaboration), "Material radioassay and selection for the XENON1T dark matter experiment," Eur. Phys. J. C **77**, 890 (2017), arXiv:1705.01828 [physics.ins-det].
22. S. Cebrián *et al.* (The NEXT collaboration), "Radiopurity assessment of the energy readout for the NEXT double beta decay experiment," JINST **12**, T08003 (2017), arXiv:1706.06012 [physics.ins-det].
23. K. Abe *et al.* (The XMASS collaboration), "Distillation of liquid xenon to remove krypton," Astropart. Phys. **31**, 290–296 (2009), arXiv:0809.4413 [physics.ins-det].
24. D. S. Akerib *et al.* (The LUX collaboration), "Chromatographic separation of radioactive noble gases from xenon," Astropart. Phys. **97**, 80–87 (2018), arXiv:1605.03844 [physics.ins-det].
25. E. Aprile *et al.* (The XENON100 collaboration), "Online ^{222}Rn removal by cryogenic distillation in the XENON100 experiment," Eur. Phys. J. C **77**, 358 (2017), arXiv:1702.06942 [physics.ins-det].
26. Y. Nakano, H. Sekiya, S. Tasaka, Y. Takeuchi, R. A. Wendell, M. Matsubara, and M. Nakahata, "Measurement of radon concentration in Super-Kamiokande's buffer gas," Nucl. Instrum. Meth. A **867**, 108–114 (2017), arXiv:1704.06886 [physics.ins-det].
27. K. Hosokawa, A. Murata, Y. Nakano, Y. Onishi, H. Sekiya, Y. Takeuchi, and S. Tasaka, "Development of a high-sensitivity 80 L radon detector for purified gases," PTEP **2015**, 033H01 (2015).
28. K. Okamoto, Y. Nakano, G. Pronost, H. Sekiya, S. Tasaka, Y. Takeuchi, and M. Nakahata, "Improvement of radon detector performance by using a large-sized PIN-photodiode," (2021), arXiv:2112.06614 [physics.ins-det].
29. Y. Nakano, K. Ichimura, H. Ito, T. Okada, H. Sekiya, Y. Takeuchi, S. Tasaka, and M. Yamashita, "Evaluation of radon adsorption efficiency values in xenon with activated carbon fibers," PTEP **2020**, 113H01 (2020), arXiv:2003.11705 [physics.ins-det].
30. Y. Kotsar, Y. Nakano, Y. Takeuchi, and K. Miuchi, "Evaluation of the radon adsorption efficiency of activated carbon fiber using tetrafluoromethane," PTEP **2022**, 023H01 (2022).
31. C. Mitsuda, T. Kajita, K. Miyano, S. Moriyama, M. Nakahata, Y. Takeuchi, and S. Tasaka, "Development of super-high sensitivity radon detector for the Super-Kamiokande detector," Nucl. Instrum. Meth. A **497**, 414–428 (2003).
32. P. Kotrappa, S. Dua, P. Gupta, and Y. Mayya, "Electret–a new tool for measuring concentrations of radon and thoron in air," Health Phys. **41**, 35–46 (1981).
33. P. Hopke, "Use of electrostatic collection of ^{218}Po for measuring Rn," Health Phys. **57**, 39–42 (1989).
34. T. Iida, Y. Ikebe, T. Hattori, H. Yamanishi, S. Abe, K. Ochifuji, and S. Yokoyama, "Electrostatic integrating ^{222}Rn monitor with cellulose nitrate film for environmental monitoring," Health Phys. **54** (1988), 10.1097/00004032-198802000-00001.
35. A. Howard, S. Carroll, and W. Strange, "A simple system for radon-in-air concentration determinations," Am. J. Phys. **59**, 544–550 (1991).
36. K. Abe *et al.* (The XMASS collaboration), "Radon removal from gaseous xenon with activated charcoal," Nucl. Instrum. Meth. A **661**, 50–57 (2012).
37. R. R. M. Gregorio, N. J. C. Spooner, J. Berry, A. C. Ezeribe, K. Miuchi, H. Ogawa, and A. Scarff, "Test of low radioactive molecular sieves for radon filtration in SF6 gas-based rare-event physics experiments," JINST **16**, P06024 (2021), arXiv:2011.06994 [physics.ins-det].
38. S. Maurer, A. Mersmann, and W. Peukert, "Henry coefficients of adsorption predicted from solid hamaker constants," Chem. Eng. Sci. **56**, 3443–3453 (2001).
39. S. Lindemann, *Intrinsic* ^{85}Kr *and* ^{222}Rn *Backgrounds in the XENON Dark Matter Search*, Ph.D. thesis, Heidelberg University (2013).
40. G. Zuzel, "Experience of gas purification and radon control in BOREXINO," in *Workshop on Low Radioactivity Techniques: LRT2017*, American Institute of Physics Conference Series, Vol. 1921, edited by D. S. Leonard (2018) p. 050001.
41. K. Pushkin *et al.*, "Study of radon reduction in gases for rare event search experiments," Nucl. Instrum. Meth. A **903**, 267–276 (2018), arXiv:1805.11306 [physics.ins-det].
42. W. Rau and G. Heusser, "^{222}Rn emanation measurements at extremely low activities," Appl. Rad. Isot. **53**, 371–375 (2000).
43. J. Hirschfelder, C. Curtiss, and R. Bird, *Molecular theory of gases and liquids*, 2nd ed. (Wiley, New York, 1954).